www.amlett.com, www.vbripress.com/aml, DOI: 10.5185/amlett.2014.3600 Published online by the VBRI press in 2014

Influence of $BiFeO_3$ addition on the electrical properties of (Na, K) (Nb, Ta)O_3 ceramic system using impedance spectroscopy

Raju Kumar, Rashmi Rani, Seema Sharma*

Ferroelectric Research Laboratory, Department of Physics, A. N. College, Patna 800013, India

*Corresponding author. Tel: (+91) 612 2260231; E-mail: seema_sharma26@yahoo.com

Received: 04 March 2014, Revised: 07 July 2014 and Accepted: 17 July 2014

ABSTRACT

Polycrystalline samples of 1- x($Na_{0.5}$ $K_{0.5}$)($Nb_{0.95}$ $Ta_{0.05}$)) -x(Bi Fe)O_3 with x=0, 0.003, 0.005, 0.007) hereby denoted as NKNT-BF were prepared by the mixed oxide method. Preliminary structural studies carried out by X-ray diffraction technique showed the formation of perovskite structure with orthorhombic symmetry. Addition of BF in the NKNT system lowered the sintering temperature by 50^0C. The nature of the frequency dependence of ac conductivity of NKNT compounds follows Jonscher power law. Complex impedance and modulus spectra confirm the significant contribution of both grain and grain boundary to the electrical response of the materials. Above the ferroelectric–paraelectric phase transition temperature, the electrical conduction is governed by the thermal excitation of charge carriers from oxygen vacancies exhibiting Negative temperature coefficient (NTCR) behaviour. Detailed study on the multiferroic properties (where magnetism and ferroelectricity are strongly coupled together) of the system is under process which is likely to form key components in the development of future technology, for example, in memories and logic devices. Copyright © 2014 VBRI press.

Keywords: Ceramics; sintering; powder diffraction; electrical conductivity.

Seema Sharma is Reader, Dept of Physics, A N College, Patna, India. She worked as Assistant Professoor at BITS Pilani-Goa campus for two years. She did her PhD in 1992 from IIT Kharagpur and did her post doctoral research at various institutes such as IIT Delhi, India, Lehigh University, Pennsylvania, USA, Manchester University, UK and IISC Bangalore, India. She has wide experience in the field of electroceramics and thin films, multiferroic nanostructured materials and Bionanomaterials. She has successfully handled sponsored and in-house research projects successfully and has published more than 80 research papers in international referred journals.

Introduction

Lead zirconate titanate (PZT) based perovskite materials have been widely used for various applications, such as piezoelectric transformers, ultrasonic motors, actuators, sensors, filters, and resonators, due to their excellent piezoelectric properties **[1–3]**. However, it is well known that PZT-based ceramics are environmentally destructive materials because of the PbO evaporation during sintering. Therefore, a study about the development of lead-free ceramics has been the most important issue to current researchers. Among all the lead-free piezoelectric materials, ($Na_{0.5}K_{0.5}$)NbO_3 (NKN) based ceramics have been extensively investigated to replace PZT because of their high-piezoelectric properties with a high Curie temperature (T_c) **[4 –7]**. However, a dense ceramic body for (Na,K)NbO_3 is difficult to obtain by ordinary sintering. In order to resolve this problem, two methods have been used. One is to develop new techniques such as hot-pressing **[8]**, spark plasma sintering **[9]** and reactive template grain growth **[10]**, but all of these techniques are relatively high in cost. The other is to modify (Na,K)NbO_3 ceramics by using dopants to form solid solutions. So far, doped materials have been grouped into two perovskite compounds (Na,K)NbO_3-$A^{+1}B^{+5}O_3$ and (Na,K)NbO_3-$A^{+2}B^{+4}O_3$. For example, (Na,K)NbO_3-$LiNbO_3$ **[11-12]** (Na,K)NbO_3-$LiTaO_3$ **[13]**, (Na,K)NbO_3- $LiSbO_3$ **[14-15]**, (Na,K, Li) (Nb,Ta,Sb,Mn) **[16]** and (Na,K)NbO_3-$BaTiO_3$ **[17]** have been studied and found to exhibit better sintering characteristics and piezoelectric properties than non-doped materials. Moreover, (Na,K,Li) (Nb,Ta,Sb) O_3 ceramics were also reported to have excellent piezoelectric properties **[18-19]**. Kosec and Kolar also presented a theory that A site vacancies in ABO_3 structure accelerate the transportation of the slowest-moving species involved in the densification process and promote the sintering process for NKN ceramics **[20]**.

$BiFeO_3$ (BF), a rhombohedrally distorted perovskite - type $A^{+3}B^{+3}O_3$ structure with the space group *R3c* has a

high Curie temperature of about 820–850^{0}C. It has been successfully applied to PZT ceramics to form a solid solution in order to lower the hot-pressing temperature and improve the piezoelectric properties **[21]**. However, this system has a large current leakage and a high coercive electric field, both of which make it difficult to become a good piezoelectric by a conventional poling process. These problems may be eased by many attempts, such as doping a few molar percent of La, Ga, and so on, or carefully controlling sintering conditions. In this study, a small amount of BF was used to partially substitute NKNT to examine its effect on the structure, dielectric and electrical properties of the ceramics. The effect of BF doping on the sintering and various electrical properties of 1-x($Na_{0.5}K_{0.5}$)($Nb_{0.95}Ta_{0.05}$)O_3-x(BiFe)O_3 (x=0, 0.003, 0.005, 0.007) ceramics have been studied in detail with the help of Impedance Spectroscopy method. The aim of the present work is to examine and optimize the electrical properties of the multiferroic ceramic system for their suitability in electronic applications.

As we know, complex impedance spectroscopy (CIS) is a non-destructive method to study microstructure and electrical properties of solids **[22]**. It enables us to evaluate the relaxation frequency (ω_{max}) of the material. The relaxation frequency of the material, at a given temperature, is only an intrinsic property of the material independent of geo-metrical factors of the sample. Consequently, an analysis of the electrical properties (conductivity, dielectric constant/loss, etc.) carried out using relaxation frequency (ω_{max}) gives unambiguous results when compared with those obtained at arbitrarily selected fixed frequencies. In this way, the impedance measurements enable us to eliminate the error, if any, due to stray frequency effects. The impedance measurements on a material give us data having both resistive (real part) and reactive (imaginary part) components. It is conventionally displayed in a complex plane plot (Nyquist diagram) in terms of the following parameters:

Complex impedance; Z' (ω) =Z''- Z' = R_S – J ω C_S,

Complex admittance; Y' (ω) = Y''+ Y' = 1,

Rp + jω C_p = G (ω) + jB (ω). (1)

Complex permittivity (dielectric constant), ε'(ω) = ε '-j ε'', where Rs and **Cs** are the series resistance and capacitance and Rp and Cp are the parallel resistance and capacitance, respectively. This analysis basically involves the display of the impedance data in different formalism and provides us the maximum possible information. The display of impedance data in the complex plane plot appears in the form of a succession of semicircles attributed to relaxation phenomena with different time constants due to the contribution of grain (bulk), grain boundary, and interface/polarization in a poly-crystalline material. Hence, the contribution to the overall electrical properties by various components in the material is separated out easily. In the case of a solid crystalline material, the physicochemical process and polarization events leading to the formation of double layer capacitors at the electrode material interface takes place in such a way that this phenomenon can be represented in terms of equivalent circuit representations by a series combination of parallel RC units. The peak of the semicircle in the complex plane plot enables us to evaluate the relaxation frequency (f_{max}) of the bulk material using the relation,

$$\omega\tau_{max} = \omega_{max} R_bC_b = 1 = 2\pi f_{max} R_bC_b = 1, \quad (2)$$

$$f_{max} = 1/2\pi RbCb, \text{ and } \tau = 1/2\pi f_{max} \quad (3)$$

where R_b, C_b, and τ refer to bulk resistance, bulk capacitance, and relaxation time respectively.

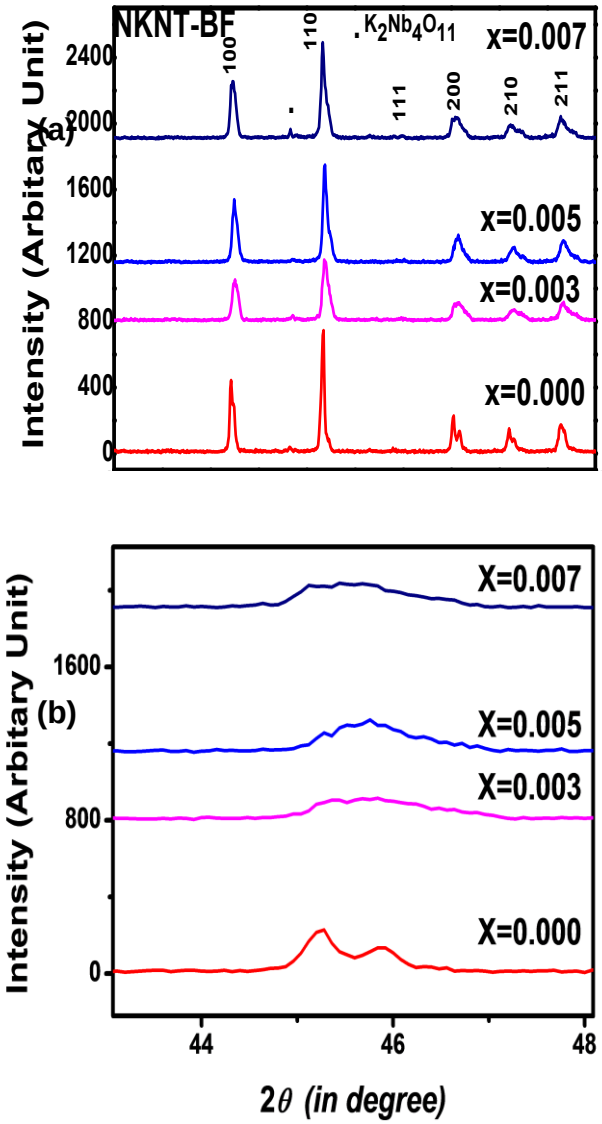

Fig. 1. (**a**) XRD of the BF doped NKNT ceramics and (**b**) enlarged XRD patterns of the ceramics for 2θ = 44-48° of different compositions x = 0.00, 0.003, 0.005 and 0.007

Experimental

Materials

NKNT-BF samples were synthesized by means of a conventional mixed oxide route. High-purity oxides and carbonates, Na_2CO_3(99.8wt%), K_2CO_3(99wt%),

Nb_2O_5(99.95wt%), Ta_2O_5(99wt%), Fe_2O_3 (99.95%), Bi_2O_3(99wt**%**) (All Sigma Aldrich chemicals, USA) were used as starting materials.

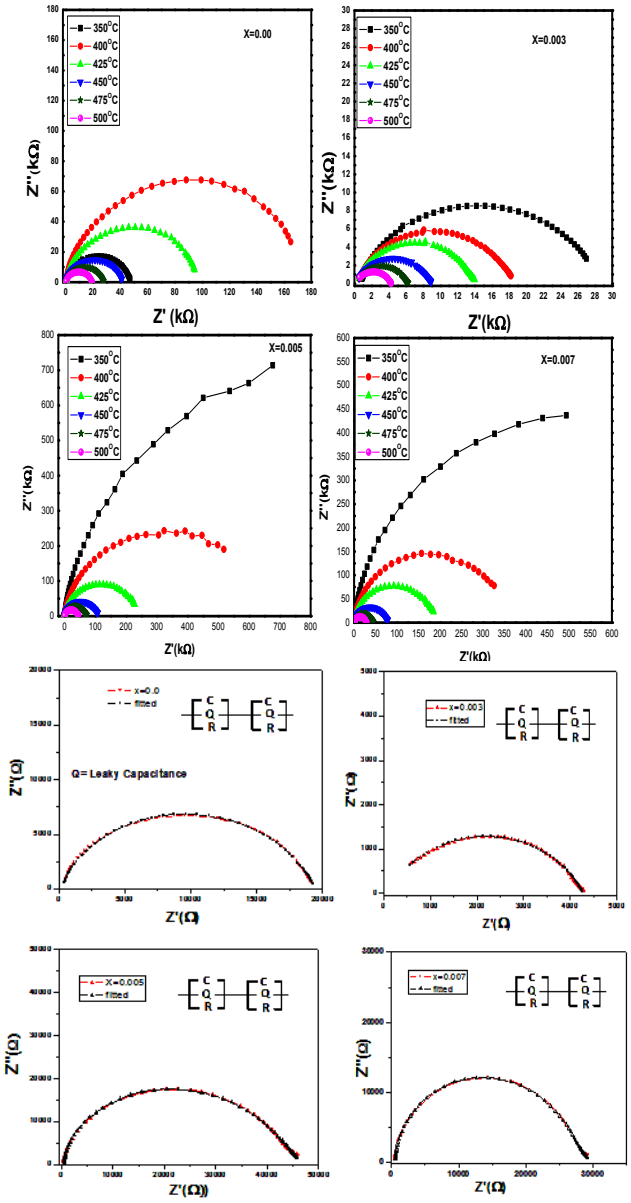

Fig. 2. Variation of real and imaginary part of impedance with temperature of pure and BF doped NKNT ceramic, (b) variation of real and imaginary part of impedance of pure and BF doped NKNT ceramic at 500 °C.

Synthesis of NKNT-BF ceramics

The powders were weighed in stoichiometric proportion and were milled for 72h in ethanol using ZrO_2 balls, and then the slurry was dried in an oven at 60°C. The calcination process was carried between 950°C- 1050°C for 2h. The synthesized powder was ball milled again for 24h in ethanol and dried, after that the powders were ground in agate mortar and pressed into pellets of 10 mm in diameter and thickness of about 2mm and then sintered between 1070 °C- 1120 °C for 24 h and cooled to room temperature. Silver paste was applied on the both the side surfaces of the samples to serve as electrodes for the electrical measurements. The crystal structure was determined using an X-ray diffractometer with a scanning rate of 0.02°/minute for 2θ in the range of 10°-80° by employing CuKα radiation (XRD-Philips Expert System) under the conditions of 50 kV and 40 mA. The identification of the peaks was carried out using the Topas 23 refinement programme. The electrical properties of the ceramics were measured as a function of frequency (1 kHz to 1 MHz) and temperature (room temperature (RT) to 550°C) using an impedance analyzer (PSM1735, UK).

Results and discussion

X-ray diffraction patterns of the NKNT system are shown in **Fig. 1(a)**. With increasing BF content, the splitting between two diffraction peaks of (002) and (200) near 45^0 gradually disappears (**Fig. 1(b)**), indicating the phase transition from an orthorhombic to a pseudocubic phase. A Morphotropic Phase Boundary (MPB) between the ferroelectric orthorhombic and the pseudocubic phase is determined to be between $0.003 \leq x \leq 0.005$.

Fig. 2 (a) shows complex impedance spectrum (Nyquist plot) of materials for different compositions. It is observed that at lower temperatures, a single semi-circular arc appears. This single semicircular arc suggests the presence of grain interior (bulk) property of the material **[23]**. However, at higher temperatures another arc appears and the spectrum comprises of two semicircular arcs with their centers lying below the real axis for all compositions. The depressed nature of semicircular arc with the center lying below real impedance axis suggests that the relaxation process is of non-ideal or non-Debye in nature. This non-ideal behavior may be originated from several factors such as the grain orientation, grain size distribution, grain boundaries, atomic defect distribution, and stress–strain phenomena etc. The presence of two semicircular arcs in the impedance spectrum of BF-substituted samples indicates the presence of both bulk and grain boundary contribution to its overall electrical property. The high-frequency curves are attributed to the bulk properties of the material which arise due to parallel combination of the bulk resistance (R_b) and bulk capacitance (C_b), where- as the low frequency semicircles are attributed to the grain boundary effects. The arc attributed to the grain boundary contribution is electrically equivalent to the parallel combination of grain boundary resistance and capacitance. The electrical equivalent circuit corresponding to the sample impedance response is shown as inset of **Fig. 2 (b)**.

The values of resistance and capacitance due to each contribution can then be evaluated from the impedance spectrum. The intercepts of the semicircular arcs with the real axis (Z') give us an estimate of the bulk resistance (R_b) of the material **[24]**. It has been observed that the bulk resistance of BF doped NKNT decreases with increase in temperature showing a typical semiconducting property, i.e. negative temperature coefficient of resistance (NTCR) behavior. It is found that the value of grain resistance decreases with rise in temperature for all the compositions.

Fig. 3 shows the variation of real part of impedance (Z') as a function of frequency (10^2–10^6Hz) at different temperatures and compositions.

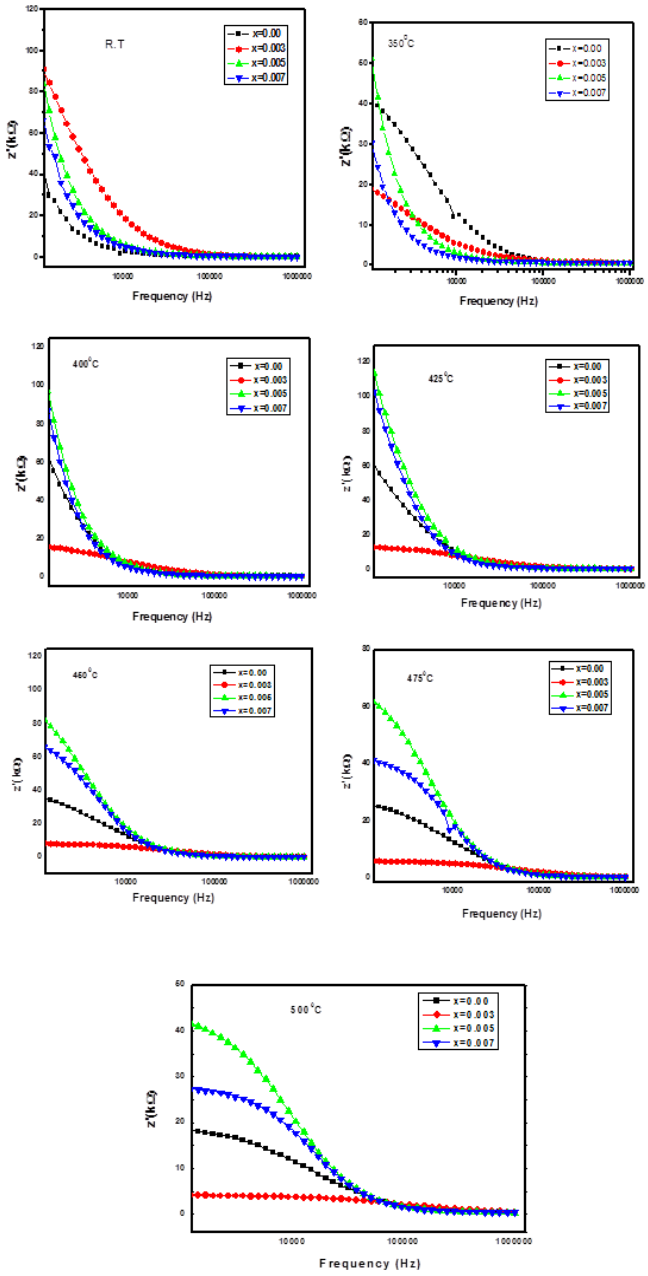

Fig. 3. Variation of real part (Z′) of pure and BF doped NKNT ceramic with frequency at different temperatures.

It has clearly been observed that Z' has higher values at lower frequencies and it decreases monotonically with increase in frequency and attains a constant value at higher frequencies irrespective of temperatures. This trend (attainment of constancy of Z' value) appears to be shifting gradually towards higher frequency side with rise in temperature. The magnitude of Z' decreases with increase in temperature and its values for all temperatures merge in the higher frequency domain. The decrement in the real part of impedance (Z') with rise in the value of temperature and frequency may be due to increase in ac conductivity with rise in temperature and frequency. The merger of real part of impedance (Z') for all temperatures in the higher frequency is due to the RC network where current passes through conducting regions in the material at low frequency and at higher frequency the current passes through insulating (capacitive) regions **[25-26]**.

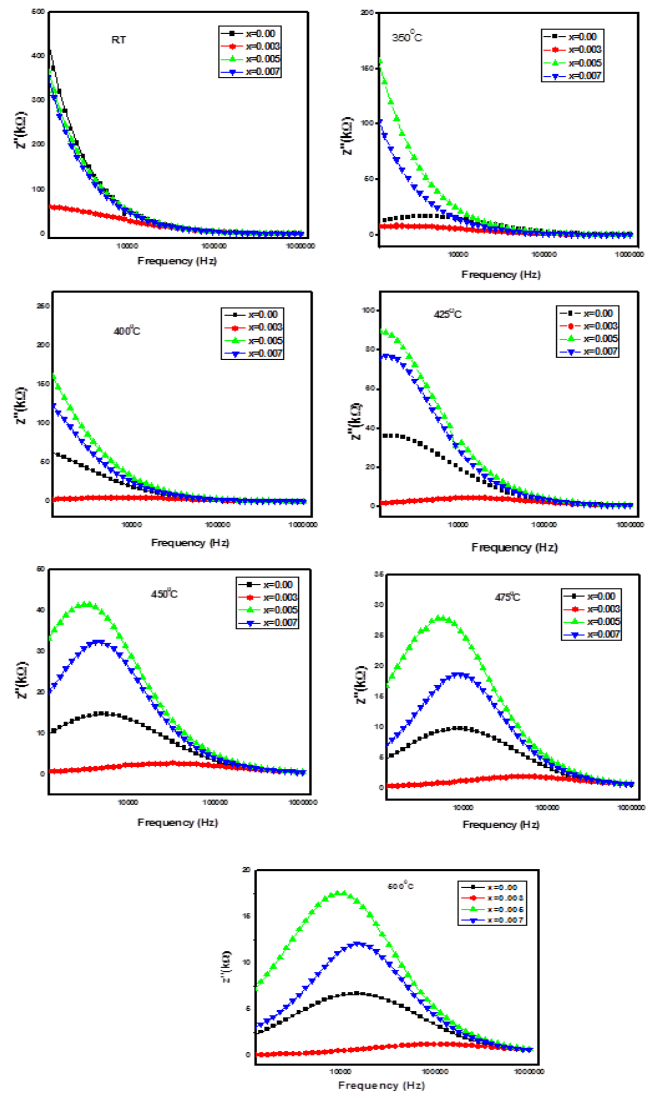

Fig. 4. Variation of imaginary part impedance (Z″) of pure and BF doped NKNT ceramic with frequency at different temperatures.

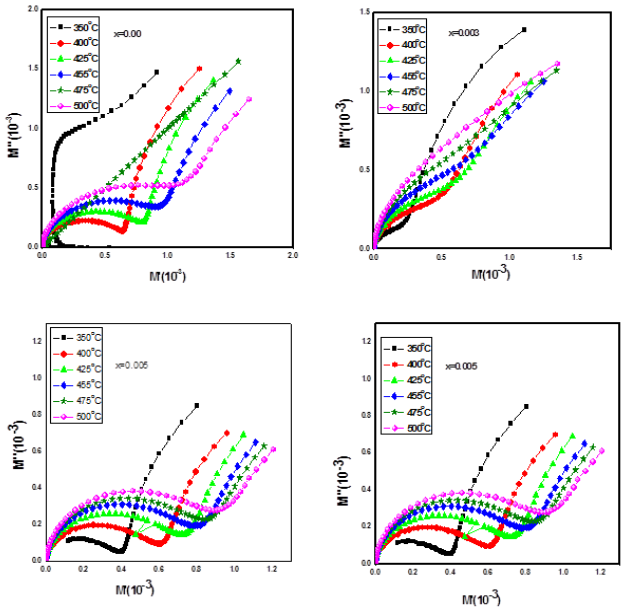

Fig. 5. Variation of real and imaginary part of modulus with temperature of pure and $BiFeO_3$ doped $NaKNbTiO_3$ ceramics.

Fig. 4 exhibits frequency and temperature dependence of imaginary part of impedance (Z'') for NKNT- BF solid-solutions. The typical variation indicates that Z'' attains a maximum value at a particular frequency, which is different for different temperatures. This variation shows a considerable decrease in the magnitude of Z'' with a shift in the peak frequency towards the higher side with increase in temperature. This feature becomes notable at higher temperature. The trend of variation of Z'' with a shift in the peak frequency is because of the presence of electrical relaxation phenomenon in the material and it is a clear proof of temperature dependent relaxation. A relative lowering in the magnitude of Z'' with a shift in the peak frequency towards the higher side with rise in temperature arises possibly due to the presence of space charge in the material. This result is in good agreement with the observation of complex impedance spectrum results **[27-28]**.

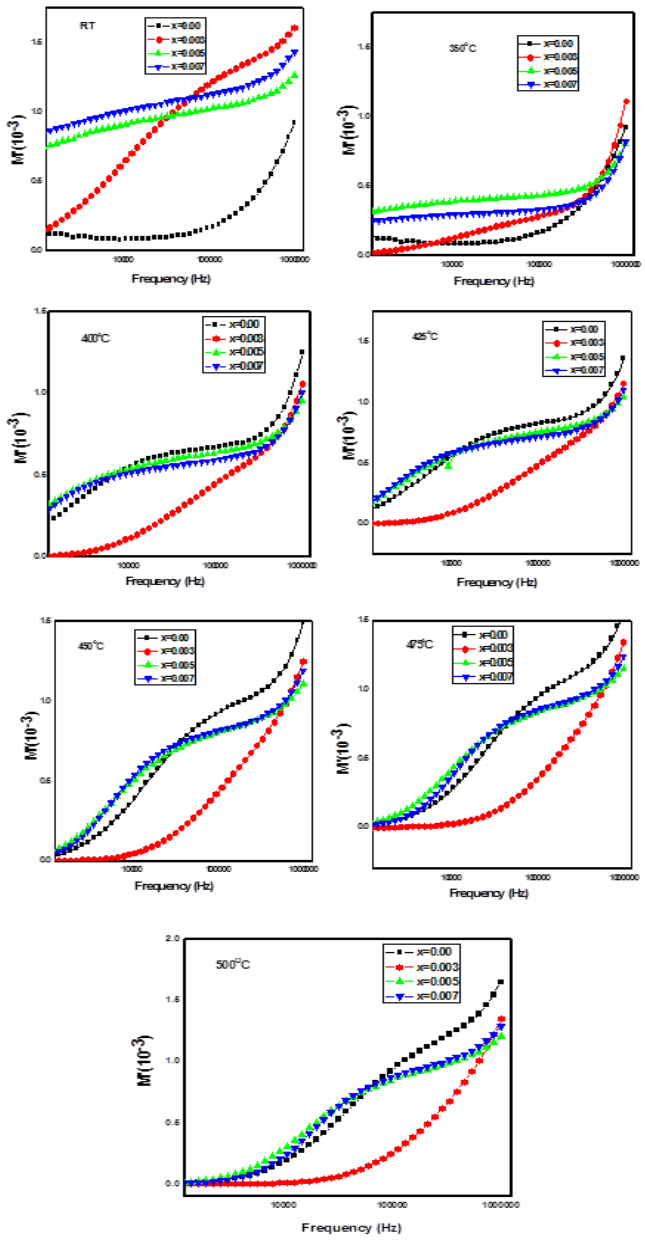

Fig. 6. Variation of real part of (M') of pure and BF doped NKNT ceramic with frequency at different temperatures.

In order to confirm the ambiguity arising in connection with the presence of grain boundary effect at elevated temperatures, the impedance data has been re-plotted in the modulus formalism at the same temperatures for $0 \leq x \leq 0.007$ (**Fig. 5**). It shows two semicircular arcs in the complex modulus plots with a small semi-circle at low frequency and large semi-circular arc in the high frequency region at all the temperatures. The pattern appears to be almost similar for both pure and BF doped NKNT. Furthermore, the modulus spectrum shows a marked change in the shape with rise in temperature suggesting a probable change in the capacitance value of NKNT material as a function of temperature.

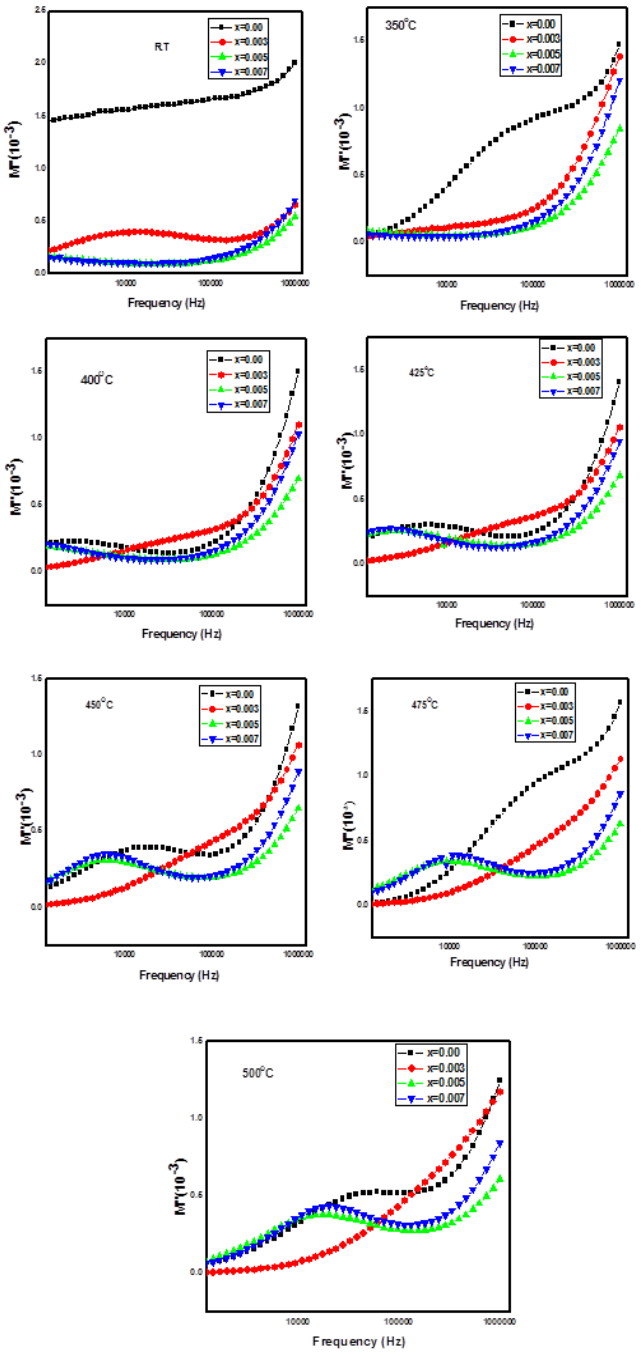

Fig. 7. Variation of imaginary part of (M'') of pure and BF doped NKNT ceramic with frequency at different temperatures.

Fig. 6 shows the variation of real part of modulus as a function of frequency at different temperatures. The variation of M' with frequency for all the samples shows a dispersion tending towards M^{∞} (the asymptotic value of M' at higher frequencies), and it (dispersion) shifts towards higher frequency side as temperature increases. Monotonous dispersion with increasing frequency at lower temperatures may have been caused by short range mobility of the charge carriers. Such results may possibly be related to a lack of restoring force governing the mobility of the charge carriers under the action of an induced electric field. The value of M' decreases with rise in temperature in the observed frequency range. **Fig. 7** depicts variation of imaginary part of modulus (M'') with frequency. It shows a broad single peak at low temperature (350 °C) in the said frequency range, above which a low temperature plateau followed by a high temperature dispersive region is observed in the pattern. The peaks are asymmetric and broader than the ideal Debye curve. The frequency range where the peaks occur is the indicative of transition from long range to short range mobility **[29]**.

The asymmetric plot of M' is because of stretched exponential character of relaxation time of the material. The stretched exponential function $\Phi(t)$ is defined by the Kohlaraush-Willium-Watts (KWW) function.

$$\Phi(t) = \exp(-t/\tau\beta) \qquad (4)$$

where $\Phi(t)$ is relaxation time of the electric field, τ is the characteristic time, and β is the relaxation parameters representative of a distribution of a relaxation times. The value of β lies in the range of $0 < \beta < 1$, which shows the departure from the linear exponential ($\beta = 1$). This behaviour shows a difference in M'' vs. frequency pattern when BF is added to the NKNT solid-solution. At low temperatures, a broad single peak is observed and its position appears to be shifting towards higher frequencies with increasing temperatures. Further, the size (height) of the modulus peak appears to increase with rise in temperature suggesting a corresponding decrease in the capacitance value with temperature. The frequency dependence of conductivity in different materials is described by power relation proposed by Jonscher **[30]**.

$$\sigma(\omega) = \sigma_{dc} + A\omega^{n} \qquad (5)$$

where σ_{dc} is frequency independent conductivity and the coefficient A and the frequency exponent n are thermally activated, material dependent quantities. The term $A\omega^{n}$ contains the ac dependence and characterizes all dispersion phenomenon. Funke **[31]** explained that the value of n might have a physical meaning; i.e., if $n \leq 1$, then charge carriers take a translational motion with a sudden hopping, when n > 1, would mean a localized hopping of the species with a small hopping without leaving the neighborhood.

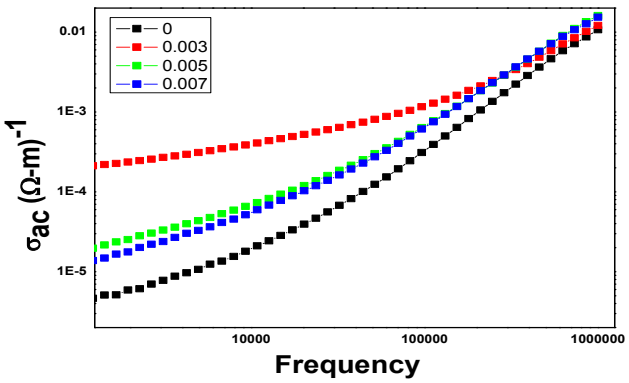

Fig. 8. Variation of polarization conductivity σac with frequency at room temperature for pure and BF doped NKNT ceramic.

Fig. 8 shows the ac electrical conductivity $(\sigma(\omega))$ as a function of frequency at room temperature. The plots showed a dispersive nature at room temperature due to the typical RC network. Low frequencies region is dominated by conductive process in the material while the higher frequency ones are dominated by capacitive region, and because of this the conductivity is almost constant and narrow **[25-26]**. The high conductivity in the material is believed to result from the high defect concentration, mainly due to oxygen vacancies generated because of substitution of BF. The large slope in this figure may be interpreted as the ac conductivity due to the hopping of the mobile species, which increases with increase in frequency (ω) and is proportional to ω^{n} given in the power relation which indicates that the electrical network (RC) response is qualitatively similar to the universal dielectric response (UDR) **[26]**.

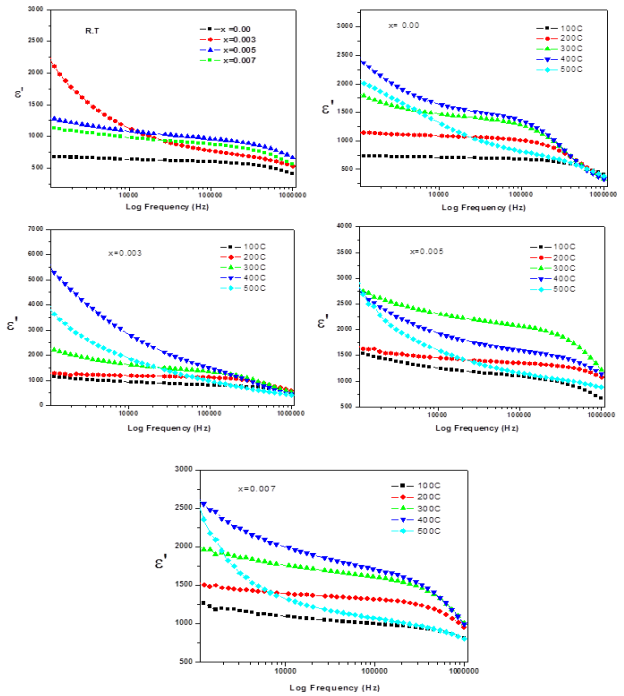

Fig. 9. (a) Plot of real part of permittivity ε' of NKNT and BF doped NKNT as a function of frequency (a) at room temperature (b) at high temperatures for different BF concentration x = 0.0, 0.003, 0.005 and 0.007.

Fig. 9 shows the relative permittivity with frequency for the NKNT and BF doped NKNT system at room temperature and different temperatures. The typical room temperature plot (**Fig. 9a**) and high temperature plots are found to be very reliable. The increase in dielectric constant ε' at low frequencies is attributed to the interfacial polarization that occurs at the boundaries separating the crystalline and non-crystalline regions, the former region having much higher resistivity. As the frequency increases the time available for the drift of charge carriers is reduced and the observed increase in ε' is substantially less. Space charge polarization at electrodes is also considered to be a contributing factor at low frequencies for the increase in ε '. The permittivity plot is the true complement of the impedance results. The observed variation of ε' with frequency can be attributed to frequency relaxation in the material. A high degree of dispersion of the permittivity is identified at high temperature (>250C) and at low frequencies (<1 kHz). This behavior is found for the dielectric materials, in which a conduction mechanism of the hopping type is present **[32]**.

Fig. 10 shows imaginary part of the dielectric permittivity (ε'') with frequency for the NKNT and BF doped NKNT system at room temperature and different temperatures. All the curves show an intense increase of the loss magnitude at increased temperature compared to their room temperature values (**Fig. 10a**). At high frequencies, the loss is much lower than one occurring at low frequencies. This kind of dependence of the ε'' with frequency is associated with the dielectric loss due to the conduction mechanism occurring at high temperatures for ceramics **[33]**.

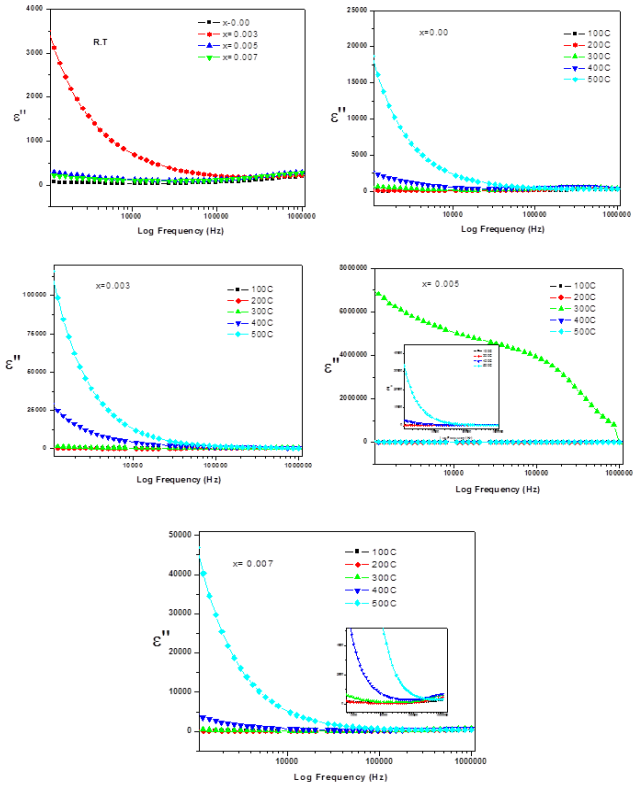

Fig. 10. (a) Plot of dielectric loss (ε'') of NKNT and BF doped NKNT as a function of frequency at room temperature (b) at high temperatures for different BF concentration x = 0.0, 0.003, 0.005 and 0.007.

Conclusion

The present work reports the result of our investigation on the dielectric and electrical properties of NKNT and BF doped NKNT prepared by high temperature solid state reaction method using complex impedance spectroscopy technique. All the samples show pure perovskite orthorhombic crystal structure. A MPB between the ferroelectric orthorhombic and the pseudocubic phase was determined to be between $0.003 \leq x \leq 0.005$. The electrical property indicates that the materials exhibit (a) at lower temperatures, a single semi-circular arc appears, it attributed to grain interior conduction (b) at the higher temperature another arc appears has been attributed to the presence of grain boundary conduction, (c) negative temperature coefficient (NTCR) behavior, and (d) temperature depend relaxation phenomena, (e) AC conductivity plots showed the high conductivity in the material is believed to result from the high defect concentration, mainly due to oxygen vacancies generated because of substitution of BF, (f) AC conductivity increases with increase in frequency (ω) and is proportional to ω^n indicating that RC network response is qualitatively similar to the universal dielectric response (UDR) , (g) The increase in dielectric constant ε' at low frequencies is attributed to the interfacial polarization (h) variation of ε' with frequency can be attributed to frequency relaxation in the material. Future prospective of this system lies with the detailed careful investigation and optimization of the multiferroic properties of this ceramic system to find their suitability in magnetic memories and electronic devices.

Reference

1. Wanders, J. W.; Piezoelectric Ceramics—Properties, Application (Philips Components, Eindhoven, **1991**).
2. Jaffe, B.; Cook, W. R.; Jaffe, H.; Piezoelectric Ceramics (Academic, New York, **1971**).
3. Yoo, J. H.; Yoo, K. H.; Lee, Y. W.; Suh, S. S.; Kim, J. S.; Yoo, C. S., Jpn.J. Appl. Phys. **2000**, *2680*, 39. **DOI:** 10.1143/JJAP.39.2680
4. Fujioka, C.; Aoyagi , R .; Takeda, H.; Okamura, S .; Shiosaki , T., J. Eur .Ceram .Soc, **2005**, *2723*, 25. **DOI:** 10.1016/j.jeurceramsoc.2005.03.129
5. Hiruma, K. Y.; Nagata, H .; Takenaka, T . Jpn., J . Appl .Phys. **2006**, *4493*, 45. **DOI:** 10.1143/JJAP.45.4493
6. Shirane ,G.; Newnham, R .; Pepinsky,R .; Phys. Rev. **1954**,*581*, 96 **DOI:** 10.1103/PhysRev.96.581
7. Cross, L.E; Ferroelectrics, **1987**, *241*, 76. **DOI:** 10.1080/00150198708016945
8. Jaeger, R.E.; Egerton; L., J. Am. Ceram. Soc, **1962**, *208*, 45. **DOI:** 10.1017/S1431927605050683
9. Shen, Zong-Yang.; Jing-Feng Ke Wang, Siyang Xu, J. Am. Ceram. Soc., **2010**, *93*, 1378. **DOI:** 10.1111/j.1551-2916.2009.03542.x
10. Saito, Y.; Takao, H; Tani1, T. Nonoyama,T.; Takatori, K.; Homma,T.; Nagaya, T.; Nakamur, M., Nature, **2004**, *432*, 84. **DOI:** 10.1038/nature03028
11. Guo, Y.; Kakimoto, K.I.; Ohsato, H., Appl. Phys. Lett. **2004**, *4121*, 85. **DOI:** 10.1063/1.1813636
12. Lévêque, G.; Marchet, P.; Levassort, F.; Tran-Huu-Hue, L.P.; Duclere, J.R., Journal of European Ceramic Society, **2011**, *31*, 577. **DOI:** 10.1016/j.jeurceramsoc.2010.10.031
13. Guo, Y.; Kakimoto; K.I, Ohsato, H; Mater. Lett, **2005**, *241*, 59. **DOI:** 10.1590/S0103-97332009000300010
14. Yang, Z.P.; Chang, Y.; Liu, B.; Wei, L.L., Mater. Sci. Eng.A. **2006**, *292*, 432.

DOI: 10.1016/j.jallcom.2009.12.052
15. Zhang, S.; Xia, R.U.; Shrout, T.R.; Zang, G.; Wang, J. , Solid State Commun. **2007**, *675*,141.
DOI:10.1088/1468-6996/9/2/025004
16. Rani, R.; Sharma, S.; Rai, R.; Kholkin, A.L., J Appl. Phys, **2011**, *104102*, 110.
DOI: 10.1063/1.3660267.
17. Lee, H.J.; Ryu, H.; Bae, M.S.; Cho, Y.K.; Nahm, S., J. Am.Ceram. Soc. **2006**, *3529*, 89.
DOI: 10.1111/j.1551-2916.2006.01197.x
18. Saito, Y.; Takao, H.; Tani, T.; Nonoyama, T.; Homma, K. T.; Nagaya, T.; Nakamura , M., Nature**. 2004**, *84*, 432.
DOI: 10.1038/nature03028
19. Zhang, Q.; Zhang, B.P.; Hai, H.T Lee; Shang, P.P., J. Alloy. Compnd. **2010**,*260*,490.
DOI: 10.1016/j.jallcom.2009.09.172
20. Kosec, M.; Kolar, D., Mater. Res. Bull. **1975**, *335*, 10.
DOI: 10.1016/0025-5408(75)90002-1
21. Kaneko, S.; Dong, D.; Murakami, K., J. Am. Ceram. Soc. **1998**, *1013*, 81.
DOI: 10.1111/j.1151-2916.1998.tb02439.x
22. MacDonald, J. R., Impedance Spectroscopy Emphasizing Solid Materials and Systems (John Wiley, Sons, New York, **1987**).
23. Tandon, R. P., J. Korean Phys. Soc. **1998**, *327*, 32.
DOI: 10.1046/j.1440-1746.1998.01750.x
24. Yemu, B., ZSIMPWIN, Version 2, Electrochemical Impedance Spectroscopy (EIS) Data Analysis Software, Princeton Applied Research, **1999**.
25. Almond, D.P., Bowen, C.R., Physical Review Letter, **2004**, *157601*, 92.
DOI: 10.1103/PhysRevLett.92.157601
26. Bowen, C.R.; Almond, D.P., Materials Science and Technology, **2006**, *719*, 22.
DOI: 10.1179/174328406X101328
27. Sen, S.; Mishra, S.K.; Das, S.K.; Tarafdar, A., J. Alloys Compounds, **2008**, *395*,453.
DOI: 10.1007/s10854-013-1172-8
28. Shukla, A.; Choudhary, R. N. P.; Thakur, A. K., J. Phy. Chem. Solids **2009**, *1401*, 70.
DOI: 10.1063/1.35491
29. Jonscher, A. K., Dielectric Relaxation in Solids (Chelsea, London, **1983**).
DOI: 10.1088/0022-3727/32/14/201
30. Jonscher, A.K., J. Mater. Sci. **1981**, *2037*, 16.
DOI: 10.1007/BF00542364
31. Funke, K., Prog. Solid State Chem. **1993**, *111*, 22.
DOI: 10.1016/0079-6786(93)90002-9
32. Sen, S.; Choudhary, R. N. P., Mater. Chem. Phys. **2004**, *256*, 87.
DOI: 10.1016/j.ceramint.2014.04.070
33. Dutta, S.; Choudhary, R.N.P.; Sinha, P.K., Eur. Phys. J. Appl. Phys. **2006**,*141*, 36.
DOI: 10.1051/epjap:2006108

